Foods and Raw Materials. 2025;13(2)

ISSN 2308-4057 (Print)
ISSN 2310-9599 (Online)

Research Article
Open Access

Available online at http://jfrm.ru/en
https://doi.org/10.21603/2308-4057-2025-2-644
https://elibrary.ru/VVDOJN

Lycopene from tomato biomass: Extraction and stabilization

Rosa Nallely Murillo Vázquez[1], Fermín Paul Pacheco Moisés[1],
Verónique Nardello-Rataj[2], Gregorio Guadalupe Carbajal Arízaga[1,*]

[1] University of Guadalajara, Guadalajara, Mexico
[2] University of Lille, Lille, France

* e-mail: gregoriocarbajal@yahoo.com.mx

Received 17.10.2023; Revised 27.02.2024; Accepted 05.03.2024; Published online 29.10.2024

Abstract:
Lycopene and other carotenoids have a significant added value in the food and cosmetic industries due to their nutraceutical properties and antioxidant activity. The extraction and stabilization of these compounds remain challenging due to their sensitivity to light, temperature fluctuations, and oxidation. This article introduces a sustainable method of extracting lycopene from tomato waste (*Solanum lycopersicum* L.) using layered double hydroxide nanoparticles to stabilize lycopene.

We used tomato juice and lycopene as a positive control, while ZnAl was a negative control. The experimental samples included 75 and 100 mg of zinc salt per 1 mL of tomato juice, which were labeled as ZnAl75J and ZnAl100J.

Zinc and aluminum salts developed insoluble hydroxides, which precipitated lycopene from tomato juice, thus forming composites. The composites proved to be efficient means of encapsulating lycopene as they recovered 97% lycopene present in tomato juice. The physicochemical properties of the organic material enhanced resistance to thermal degradation and acted as an extended-release antioxidant. ZnAl100J, which contained a lot of lycopene, inhibited 89% of DPPH$^{\bullet}$ in 24 h and showed a value higher than IC$_{50}$ for ABTS$^{\bullet+}$, which was 0.02 μg/mL of TEAC ABTS$^{\bullet+}$. ZnAl75J composites showed a higher protection against oxidation and a higher sun protection factor value (3.08) at 15% concentration.

The composites could be used as an active ingredient in a wide range of formulations that require antioxidant and photosensitizing properties, or simply as encapsulators and carriers of lycopene.

Keywords: Lycopene, composites, hydroxides, zinc salts, aluminum salts, layered nanoparticles, antioxidant activity

Funding: This research was supported by the National Council for Humanities, Sciences, and Technologies (CONAHCYT), México, due to the doctoral scholarship given to Rosa Nallely Murillo Vázquez (CVU number: 486681).

Please cite this article in press as: Murillo Vázquez RN, Pacheco Moisés FP, Nardello-Rataj V, Carbajal Arízaga GG. Lycopene from tomato biomass: Extraction and stabilization. Foods and Raw Materials. 2025;13(2):330–340. https://doi.org/10.21603/2308-4057-2025-2-644

INTRODUCTION

Lycopene is a nutraceutical ingredient that helps prevent diseases or minimize their symptoms. As an excellent antioxidant, it is highly demanded in the cosmetic industry. Tomatoes, which are cultivated worldwide, are extremely rich in lycopene and serve as the main source of this valuable substance [1]. Even tomato waste may be used as raw material [2, 3]. In fact, tomato waste biomass can generate lycopene, a high-value-added ingredient, to be used as a nutraceutical or cosmetic [4]. However, isolated lycopene has a major disadvantage: it degrades easily when exposed to light and ambient oxygen.

Our research team has already reported that tomato juice can be used as a reaction medium to produce layered double hydroxide nanoparticles and a composite that could serve as a carrier powder for lycopene [5]. Layered double hydroxide particles are crystalline particles with a layered structure containing a combination of M(II) and M(III) cations coordinated by hydroxyl groups. The M(III) cation generates an excess charge in the layers that is balanced with interlayer anions. As a result, a layered double hydroxide particle represents a stacking of layers of metallic hydroxides that retain interlayer anions [6, 7]. Considering that various elements can form layered double hydroxide, those with low toxicity can be selected to design particles to be used in food or cosmetics [8]. For instance, we used $Mg_3Al(OH)_8(CO_3)_{0.5}\cdot XH_2O$ [5]. Zinc and aluminum are also widely studied for layered double hydroxide formulations in pharmacy and cosmetics [9–11]. This variant is useful for topical applications in cosmetics. In this study, we reported an experiment modification of crystalline layered double hydroxide formation with $Zn_3Al(OH)_8(CO_3)_{0.5}\cdot XH_2O$ composition in tomato juice. However, our modification resulted in amorphous compounds that possessed the same efficiency in lycopene removal and stabilization.

The research objective was to study the properties of the material and determine its application in the food industry, food packaging, or cosmetics.

STUDY OBJECTS AND METHODS

We used the coprecipitation technique to synthesize the composites. First, we dissolved zinc and aluminum salts in 100 mL of tomato juice and alkalinized them with NaOH 1 M to reach pH 8.5. After that, we dissolved sodium carbonate in 20 mL of water and added it to the suspension. After stirring the suspension for 2 h at room temperature and air atmosphere, we centrifuged it at 1380 rpm, washed the red solid with water until the washing liquid reached the desired pH, and dried at 50°C. Table 1 illustrates the samples and reagents involved. As a positive control, we used tomato juice and lycopene. The ZnAl sample, which contained zinc and aluminum cations, was a negative control. ZnAl75J and ZnAl100J were the samples with 75 and 100 mg of zinc salt used per milliliter of tomato juice.

To calculate the yield percentage, we used the final weight of the dry composites as in Eq. (1):

$$\mathrm{W} = \frac{\left(W_{\mathrm{f}} \times 100\right)}{W_{\mathrm{o}}} \tag{1}$$

where W is the percentage of weight, %; W_{f} is the final weight of the dry composites; and W_{o} is the expected theoretical weight considering the inorganic phase corresponded to layered double hydroxide particles.

The X-ray diffraction profiles were collected from 100 mg of the sample pressed onto a holder to produce a smooth surface. The procedure involved a D8 ADVANCE Bruker analytical diffractometer with Cu-Kα radiation. The data were collected within the 5–70° range in 2-Theta mode with steps of 0.02° and scanned at 30 s per step. The X-ray photoelectron spectra were obtained in a SPECS spectrometer with an 1D DLD detector with a Phoibos 150 analyzer. The device employed AlKα radiation (1486.7 eV) generated at 250 W and 12.5 kV; the spectra were collected at a pressure $\leq 2.12\times10^{-9}$ mbar. The charge of operation was adjusted at 20 µA of emission and 2 eV. The samples were applied on glass. The infrared spectra were obtained from 2 mg of sample with an iS50 ATR Thermo Scientific spectrometer. The spectra were collected with 15 scans with a resolution of 4 cm^{-1} at room temperature. The scanning electron microscopy analysis involved a JEOL JSM 5400 LV microscope. The images were obtained using secondary electrons generated with a voltage of 20 kV. The energy dispersive X-ray spectroscopy maps were acquired with an X-Max detector (Oxford Instruments) at 20 mm^2, which was assembled to a JEOL JSM-6610LV microscope at 15 kV. The dynamic light scattering required 2 mg of each sample added to 2 mL of 0.9% NaCl solution and 0.1M HCl. The suspensions were dispersed with ultrasound for 10 min. The hydrodynamic size and the zeta potential were measured with a Nano ZS Malvern device. A refractive index of 1.2 was loaded to the software with 15 readings per sample. The Discovery thermogravimetric device included 2 mg of each sample at 25–900°C with steps of 20°C per 1 min under a nitrogen flow of 20 mL/min.

Quantification of lycopene content in composites. To quantify the amount of lycopene contained in the composites, we performed a solvent extraction using 5 mL toluene per 1 g composite, which was then agitated for 30 min at 1500 rpm. After that, the samples were centrifuged, and the supernatant was read in a Cary 60 UV-Vis spectrometer (Agilent Technologies) within the range of 50–500 nm. The reads were interpolated with a calibration curve.

Antioxidant activity. A stock solution of 2,2-diphenyl-1-picrylhydrazyl ($\mathrm{DPPH}^{\bullet}$) was prepared as follows. A solution of 20 mg of $\mathrm{DPPH}^{\bullet}$ in 300 mL of ethanol was agitated for 10 min, after which we measured its initial absorbance at 517 nm and verified that the read stayed below 3.0 absorbance units. Then, we weighed about 70 mg of the samples in 2 mL Eppendorf tubes and poured 1 mL $\mathrm{DPPH}^{\bullet}$ solution into each tube, leaving the samples to incubate for 30 min in the dark [12]. After that, we centrifuged the samples to ensure sedimentation of the powders and immediately measured the absorbance in a Perkin Elmer Lambda EZ 150UV-vis spectrometer. To quantify the percentage of the remaining $\mathrm{DPPH}^{\bullet}$, we used Eq. (2):

$$\%\ \mathrm{DPPH}^{\bullet} = \frac{A_{\mathrm{f}}}{A_{\mathrm{i}}} \times 100 \tag{2}$$

Table 1 Samples used to synthesize composites

$ZnCl_2\cdot6H_2O$, g	$AlCl_3\cdot6H_2O$, g	Na_2CO_3, g	Medium, 100 mL	Final weight expected, g	Sample
–	–	–	Tomato juice	3.86	Tomato juice
5.25	3.10	1.59	Water	5.00	ZnAl
–	–	–	–	0.50	Lycopene
7.88	4.65	2.39	Tomato juice	11.36	ZnAl75J
10.50	6.20	3.19	Tomato juice	13.86	ZnAl100J
0.53	0.31	0.16	Lycopene	1.00	ZnAlLyc

where A_f is the stands for the final absorbance of each sample; and A_i is the corresponds to the initial absorbance of DPPH$^•$.

We assessed the antioxidant kinetics with DPPH$^•$ by placing 50 mg of particles in 20 mL tubes, which had been protected from light with aluminum foil. In this experiment, the stock solution was diluted to set the absorbance at 0.8 units. After that, we added 10 mL of the DPPH$^•$ diluted solution to each tube and agitated them. The UV-Vis measurements were carried out in 0, 5, 15, 30, 60, 90, 90, 123, 180, 240, 360, and 1440 min in triplicate. With the values obtained, the percentage of inhibited DPPH$^•$ in the solution was calculated as follows:

$$\%\ \text{inhibition DPPH}^{\bullet} = \frac{(A_o - A_s)}{A_o} \times 100 \qquad (3)$$

where A_o is the initial absorbance of DPPH$^•$ without antioxidant added and A_s is the absorbance of the sample.

A solution of ABTS$^{•+}$ (2,2'-azino-di-3-ethyl-benzthiazoline sulphonate) in ethanol was prepared with an absorbance of 0.740 ± 0.050 at a wavelength of 732 nm. Separately, we weighed 10.0 ± 0.5 mg of each sample in Eppendorf tubes in triplicate. Then, we added 1 mL of ABTS$^{•+}$ solution to each sample and left for incubation for 5 min to take time readings in triplicate at a wavelength of 732 nm. The inhibition of ABTS$^{•+}$ was calculated according to Eq. (4):

$$\%\ \text{inhibition ABTS}^{\bullet+} = \frac{(A_o - A_s)}{A_o} \times 100 \qquad (4)$$

where A_o is the initial absorbance of the ABTS$^{•+}$ solution (0.740 ± 0.050) and A_s is the absorbance of the sample.

Antioxidant capacity on copper (CUPRAC method). This experiment involved three solutions: $NH_4(CH_3COO)$ buffer (pH = 7.1), $CuCl_2$ (10 mM), and neocuproine (7.5 mM in ethanol). In this order, 0.33 mL of each solution was added to each vial; the samples were shaken and left for incubation in the dark for 30 min. After that, the liquid part was extracted and read using the UV-Vis spectrometer at 450 nm. Each test was done in triplicate.

RapidOxy oxidation stability test. The RapidOxy assay was conducted with 0.01, 0.03, and 0.05 g of each sample added to 1 mL of purified linseed oil. After homogenization, we placed the mix in Teflon capsules inside a PetrOXY 13-3006 device to measure the induction period and the oxidation stability until reaching $\Delta PO_2 = 50\%$. The oxygen consumption, mol, was calculated using Eq. (5):

$$\text{Oxygen Consumption} = \frac{\left[P(O_2)_{max} - P(O_2)_t\right] V(O_2)}{R\,T} \qquad (5)$$

where $P(O_2)_{max}$ is the maximal pressure of O_2 inside the equipment chamber; $P(O_2)_t$ represents the pressure of O_2 upon reaching ΔP of 50%; $V(O_2)$ is the volume of O_2 contained inside the equipment chamber; R corresponds to the universal constant of perfect gases (8.314 J/(K·mol); and T is the temperature of the system at $P(O_2)_t$.

Evaluating the solar protection factor. This part of the experiment required a neutral moisturizing cream, 1 mL of which was placed in a test tube followed by three different particle concentrations: 5, 10, and 15%. This mix was centrifuged at 13 000 rpm for 3 min using an IKA T18 digital Ultra Turrax homogenizer.

The solar protection factor was measured using a Cary 60 UV-Vis device (Agilent Technologies) within the range of 290–320 nm. According to the prescribed procedure, 2 mg/cm^2 of the mix was weighed on a 1×2 cm quartz plate and dispersed, leaving a homogeneous layer. This layer was placed in the UV-Vis device to take the corresponding readings.

The absorbance readings made it possible to calculate the solar protection factor value:

$$\text{Solar protection factor} = CF \sum_{290}^{320} EE(\lambda)\, I(\lambda)\, ABS(\lambda) \qquad (6)$$

where CF is the correction factor of 10, $EE(\lambda)$ is the erythema effect spectrum, $I(\lambda)$ defines the solar intensity spectrum, and $ABS(\lambda)$ stands for the absorbance of the sample. The experiment was performed in triplicate.

RESULTS AND DISCUSSION

Figure 1 presents yields of the products and their relationship with their theoretical yield, considering that all the organic matter from the tomato juice was removed by the idealized layered double hydroxide of ZnAl (Table 1). The lyophilized tomato juice produced 3.86 g of powder, considered as 100% of the organic matter. The reference ZnAl had a yield of 60.5%, which is common when the synthesis is conducted at pH 8.5, according to our personal observations. The composites, ZnAl75J and ZnAlLyc, had a yield of 50.67 and 50.30%, respectively. ZnAl100J had the highest yield (72.84%), indicating that the yield was proportional to the amount of the salts added. Another cause of the low yield was

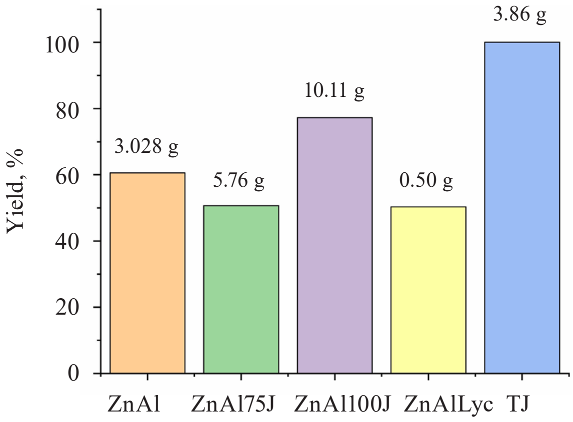

Figure 1 Solid yield obtained considering the mass of the tomato juice and the total formation of the ideal layered double hydroxide of ZnAl. TJ is tomato juice

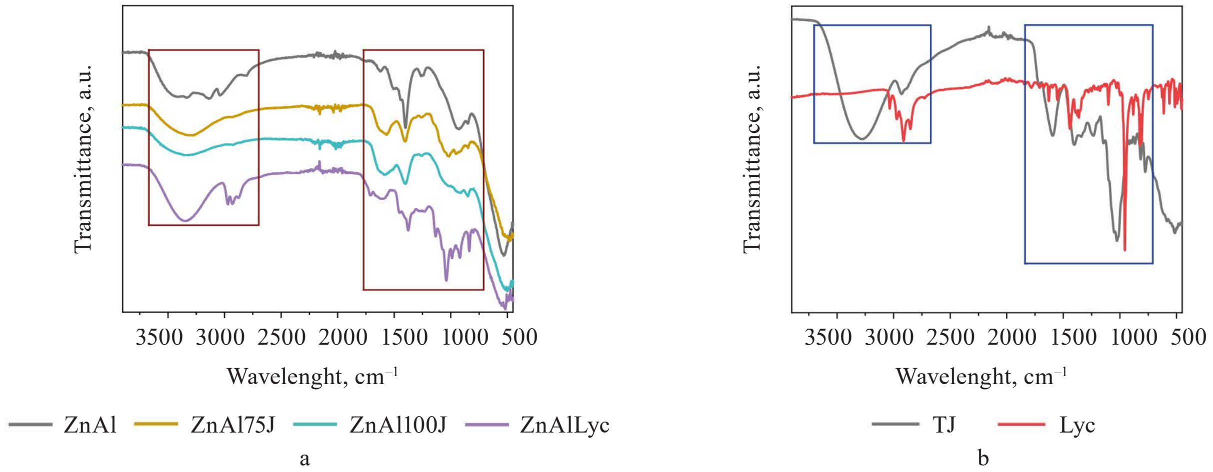

Figure 2 Infrared spectra of: the composites (a) and tomato juice and lycopene (b)

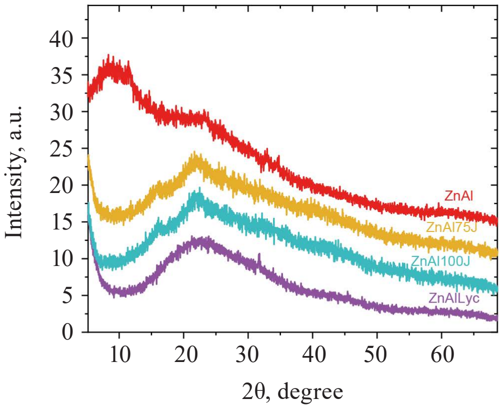

Figure 3 X-ray diffraction pattern of composites synthesized using tomato juice as reaction medium

that the expected layered double hydroxide structure was not obtained (see the X-ray diffraction section).

Figure 2 shows the infrared spectra of the composites and their respective references, i.e., tomato juice and lycopene. They exhibited bands between 3090 and 2800 cm^{-1}, which is typical of lycopene methyl groups. The band at 3400 cm^{-1} was attributed to the stretching of O-H hydroxyl bonds while the band at 994 cm^{-1} corresponded to C-H vibrations, and the band at 820 cm^{-1} was related to lycopene vinyl bonds (R2-C=C-R) [13, 14].

Regarding the composites ZnAl75J and ZnAl100J, the weak band at 1630 cm^{-1} could be attributed to the water (H_2O) bending vibration. The band at 1027 cm^{-1} corresponded to C-O stretching, and the bands at 550 cm^{-1} were attributed to the M-O groups, corresponding to Al-O or Zn-O. Another phenomenon was registered in the region around 1460 cm^{-1} and manifested itself as an increase in the signal of methyl groups combined with the carbonyl signal [15]. This information suggested the possible presence of lycopene in both composites.

The band at around 1365 cm^{-1} could be attributed to the asymmetric stretching mode of the carbonate, as confirmed by the bands at 870 and 680 cm^{-1}, which corresponded to weak bending and angular bending modes of the carbonate, respectively [16, 17]. In the ZnAl spectrum, we observed signals related to O-H stretching at 3440, 3330, and 3144 cm^{-1}, which were probably associated with water or metallic hydroxides [18].

The diffractograms of all the products showed broad signals (Fig. 3), indicating that the structure of the ZnAl reference and the composites were predominantly amorphous. A weak but clear signal was recorded at 14.4°, which coincided with the most intense signal of boehmite, i.e., AlO(OH), as described in the International Centre for Diffraction Data, 83 by 1505. Although this weak signal was the only evidence of crystalline particles, other zinc and aluminum compounds might have been formed in an amorphous phase. We performed an elemental analysis by energy-dispersive X-ray spectroscopy to identify them. The spectra revealed the presence of Zn, Al, C, and O in the sample, consistent with the presence of boehmite as confirmed by X-ray diffraction, carbonates in agreement with the IR spectrum, and zinc, probably amorphous. The composites ZnAl75J and ZnAl100J rendered the same results, indicating the presence of presumably amorphous zinc. Other elements detected were C, O, P, Na, and Cl, which corresponded to the elements from the tomato juice. In all cases, the elements were uniformly distributed throughout the matrix, as indicated by the energy-dispersive X-ray spectroscopy maps (Fig. 4). The formation of ZnAl layered double hydroxide was affected by the initial reagents, pH, and even temperature, as reported in [19]. Unlike our previous work, here we started with chloride salts instead of nitrate, with the aim of using reagents authorized for the food and cosmetics industry. Although the composites were amorphous, they were even better at developing fine powders which could be easily dispersed in the sun protection factor assays. The X-ray photoelectron spectra (Fig. 5) provided detailed information about the spectra of the Zn2p levels, indicating the presence of two types of zinc atoms in the ZnAl reference and the composites. One signal at 1020.9 eV and another at 1026.0 eV, both with a spin-splitting of

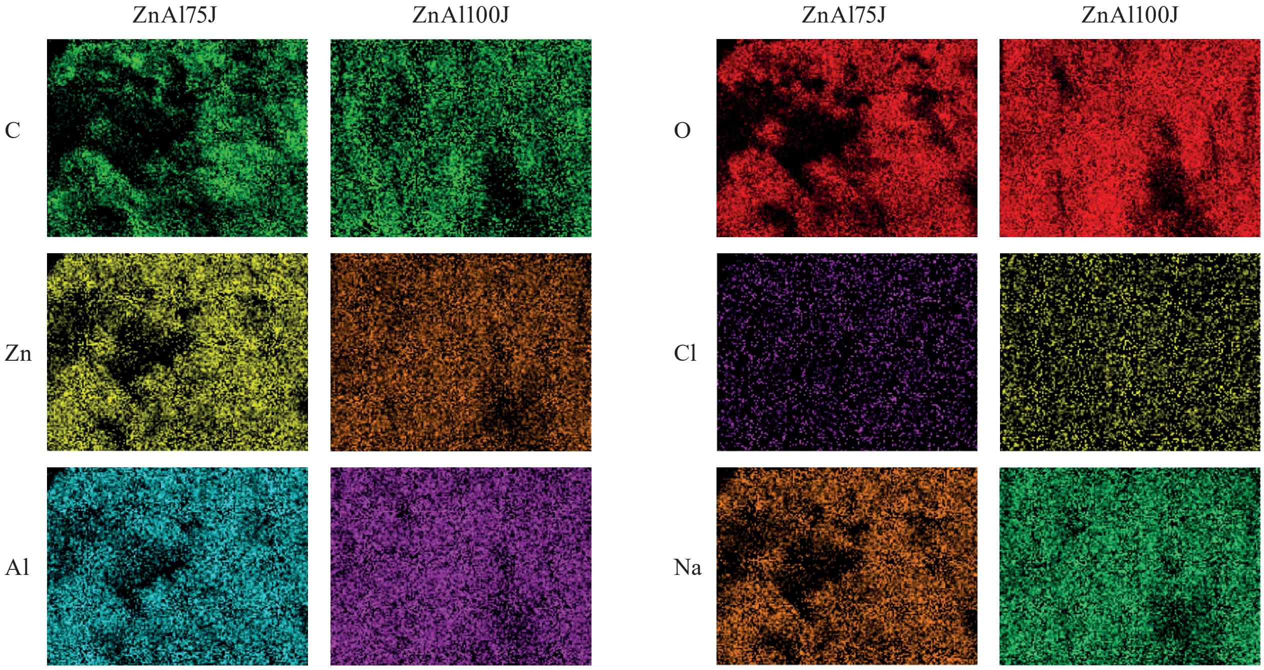

Figure 4 Elemental composition maps obtained by electron dispersive spectroscopy in composites

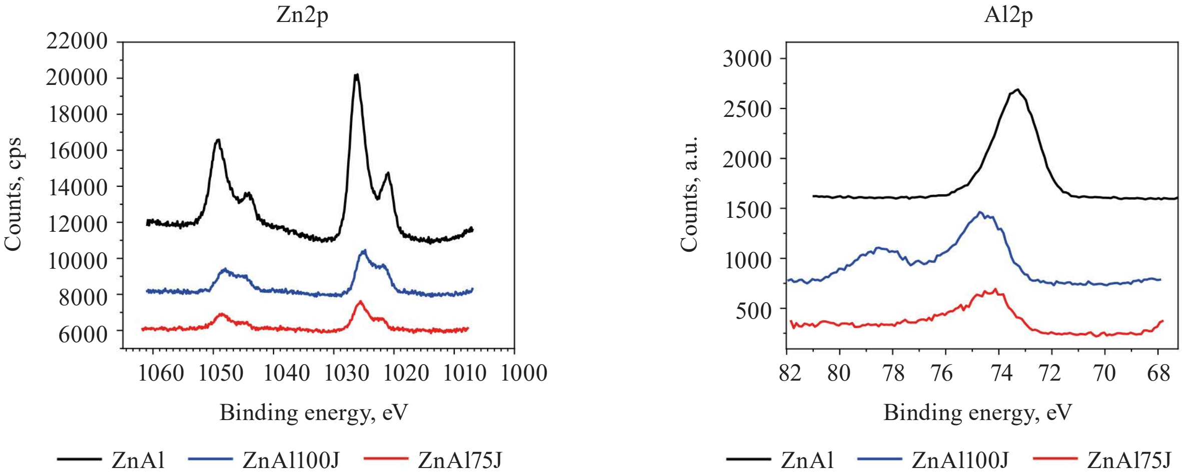

Figure 5 X-ray photoelectron spectra of Zn2p and Al2p in composites vs. ZnAl reference

23.1 eV, corresponded to Zn^{2+}, commonly found in ZnO and $Zn(OH)_2$ [20]. The signal at 1020.9 eV is typical of crystalline or amorphous ZnO [21, 22]. The signal at 1026.0 eV has not been reported in scientific literature. However, it was close to high values in salts with highly electronegative counterions, e.g., halides and sulfates, suggesting that Zn^{2+} may be attributed to anions present in tomato juice [23]. On the other hand, the Al2p spectrum of the ZnAl reference contained a signal at 73.3 eV, which is characteristic of aluminum oxides or hydroxides [23]. The composites also demonstrated a shift to 74.2 eV, consistent with the spectrum reported for aluminum hydroxide, which supported the X-ray diffraction data [24]. ZnAl100J exhibited an additional signal at 78.5 eV. Although it was not registered in databases, it approached the binding energy reported for Al with halides hydroxides, suggesting coordination with such highly negatively charged anions as Cl [23]. Therefore, the powders consisted of organic compounds from tomato pulp and amorphous zinc, aluminum oxides, or hydroxides.

The scanning electron micrographs of all the composites (Fig. 6) demonstrated ZnAl, ZnAl75J, and ZnAl100J with a rough surface and multiple cavities. Additionally, a more spherical morphology was present in clusters with smooth surfaces. The absence of defined crystalline structures could be indicative of a higher amount of organic or amorphous material, as detected by the X-ray diffraction. ZnAlLyc demonstrated different structures in the form of layers corresponding to aluminum hydroxides [25, 26]. In all cases, particles tended to be spherical in ZnAl, ZnAl75J, and ZnAl100J, while ZnAl-

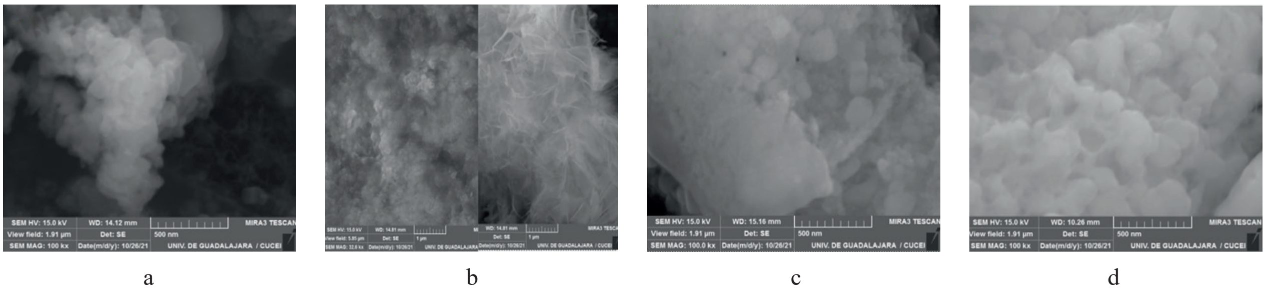

Figure 6 Micrographs obtained by scanning electron microscopy: (a) ZnAl, (b) ZnAlLyc, (c) ZnAl75J, and (d) ZnAl100J

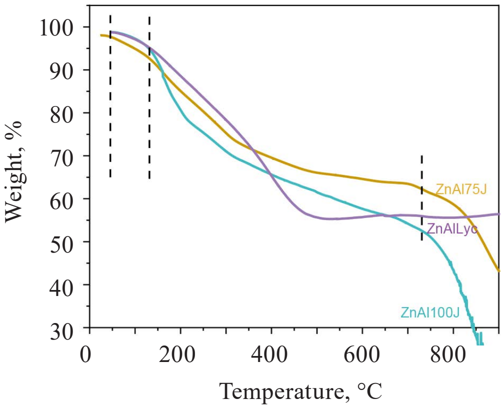

Figure 7 Thermogravimetric analysis for composites ZnAl75J, ZnAl100J, and ZnAlLyc

Lyc formed needle-like structures. All particles were 400–800 nm in size; however, the particle size in the liquid medium was different (see the dynamic light scattering section).

Thermogravimetric analysis. Figure 7 illustrates the decomposition of the composites as a function of temperature. Regarding ZnAlLyc, the degradation was continuous with the first step at 250°C and the second at 450°C. The first event might correspond to the removal of water and the burning of organic matter whereas the second event might correspond to the decomposition of metal hydroxides, possibly producing oxides at ≥ 500°C. The 50% of compounds that did not degrade could be metallic oxides of amorphous nature as they were not observed in the X-ray diffraction analysis.

ZnAl75J and ZnAl100J revealed a step that culminated at 150°C due to evaporation of approximately 5% water [26, 27]. That step was followed by another event ending at 200°C, which probably corresponded to the combustion of organic material and partial dihydroxylation. The third step was at 330–750°C, where the combustion of organic matter and the formation of metal oxides were completed [27].

Comparing the degradation profile with our previous composites with layered double hydroxide phases, this profile formed a lower slope, which indicated a slower degradation [5]. In addition, the amorphous phases in the current work provided a slightly greater thermal stability.

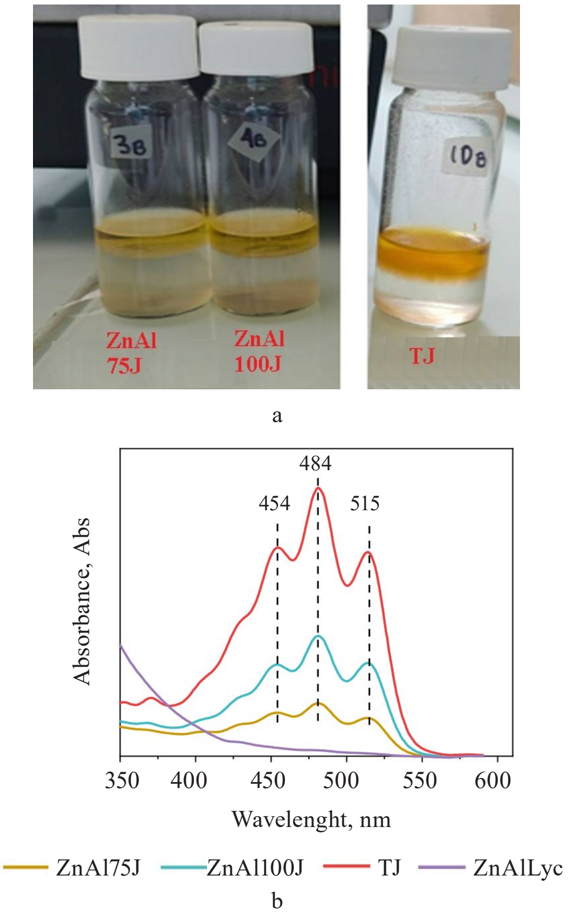

a

b

Figure 8 Extraction of encapsulated lycopene in composites (a) and UV-Vis spectra of lycopene extracted from composites with toluene (b). TJ is tomato juice

Quantification of lycopene. The quantification was possible due to the easy release of lycopene from the composites (Fig. 8a) because adsorption forces between the metal-organic composition in these composites were not strong enough to prevent organic solvents from removing lycopene with simple agitation. Figure 8a shows the red phase containing lycopene. The identification was done by comparing the UV-Vis absorption profile of the red pigment released by the samples with a standard lycopene solution (Fig. 8b), with peaks at 454, 484, and 515 nm [28]. The easy release may suggest that the nanoparticles somehow broke the pericarp and chromoplasts to let the lycopene out.

Using the quantified lycopene in tomato juice as a reference, we compared it with the lycopene released from the composites to determine recoveries per volume of tomato juice and yield. The ZnAl100J composite recovered 0.717 mg per 1 mL of tomato juice (Fig. 9a), and this amount corresponded to the yield of 95.92% (Fig. 9b). This value exceeded the highest values reported in [29, 30], which ranged between 0.43 and 0.50 mg/mL of tomato juice. ZnAl75J recovered only 26.6% of the lycopene, suggesting that the synthesis conditions of ZnAl100J require additional research.

Hydrodynamic particle size. We used a liquid medium to study the particle size of the composites because liquid is a more representative environment for their use, e.g., in foods or cosmetics. The hydrodynamic size detected by the dynamic light scattering test (Fig. 10) for ZnAl75J was 615 nm while that for ZnAl100J it was 1720 nm. Comparing these results with the scanning electron micrographs, ZnAl75J particles were completely dispersed in water. However, the aggregation was two particles on average for ZnAl100J.

Regarding the zeta potential, the composites were subjected to acidic and saline media. Figure 11 shows that the ZnAl particles maintained the positive potential in HCl and saline solution while the composites with tomato juice changed the values to negative when they were in saline solution. The positive values in HCl suggested that H^+ ions were adsorbed on the surface of the composites while Cl^- ions were retained in saline solutions. Stable suspension preparation often requires high values of the zeta potential, e.g., ≥ ± 30 mV [31]. However, the low aggregation detected by the dynamic light scattering indicated that these types of composites were easily dispersible in liquid formulations.

Antioxidant capacity. Figure 12 presents the results of total antioxidant capacity expressed as a percentage of DPPH· inhibition in 2 and 24 h. In 2 h, the inhibition was 31% for ZnAl75J and ZnAl100J. ZnAl showed 18% inhibition, which seemed to have a significant contribution from the inorganic particles. In ZnAlLyc, the inhibition slightly increased to 42% whereas the tomato juice and lycopene references showed superior activity of ≥ 90%. This phenomenon indicated that the antioxidant components in tomato juice and lycopene were more available in 2 h than those in all the composites. However, the activity of the tomato juice and lycopene

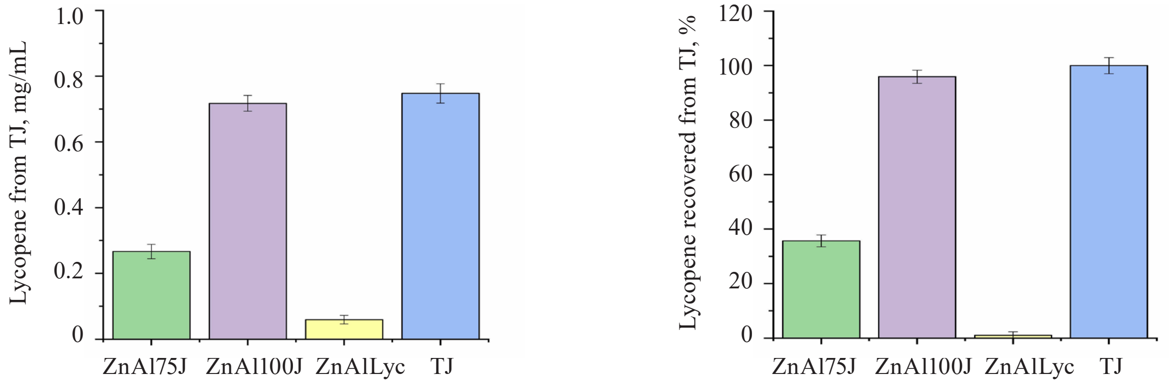

a

b

Figure 9 Lycopene recovered from tomato juice (a) and corresponding yield regarding the lycopene in tomato juice as reference (b). The bars correspond to standard deviation. TJ is tomato juice

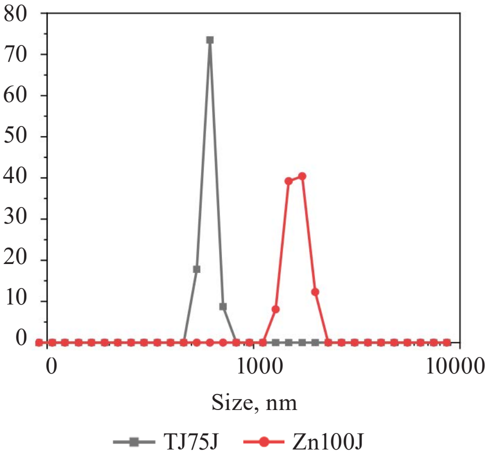

Figure 10 Dynamic light scattering test: particle size histogram

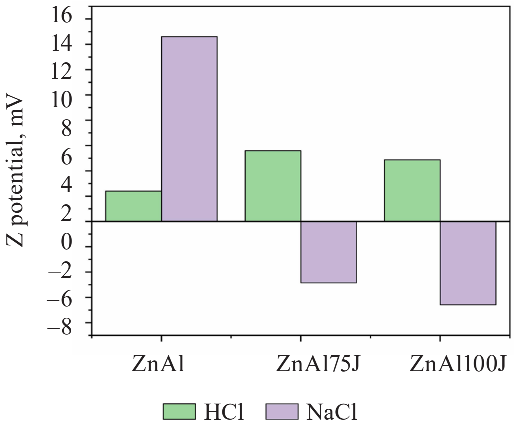

Figure 11 Zeta potential for composites in acidic (green) and saline (purple) media. TJ is tomato juice

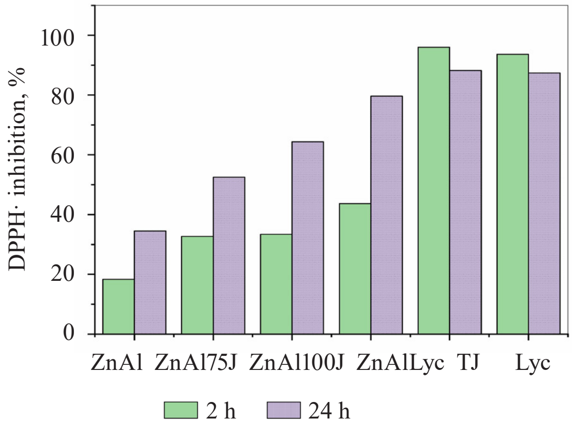

Figure 12 Percentage of DPPH$^•$ inhibition in 2 and 24 h (standard deviation ≤ ± 0.05, n = 3)

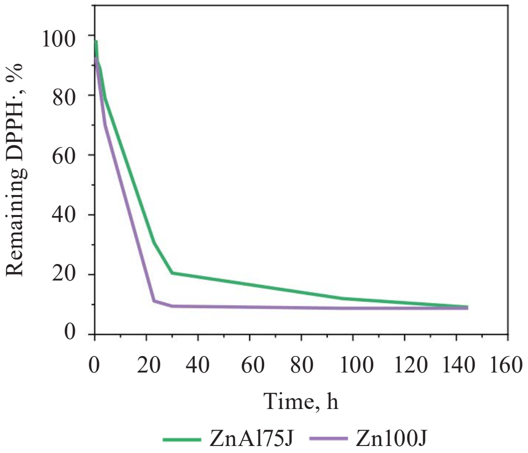

Figure 13 Percentage of remaining DPPH$^•$ over time (standard deviation ≤ ± 0.08, n = 3)

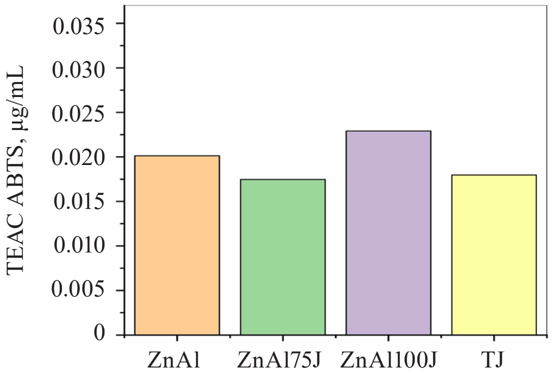

Figure 14 Trolox equivalent antioxidant capacity (TEAC) in the ABTS$^{•+}$ assay (standard deviation ≤ ± 0.05, n = 3)

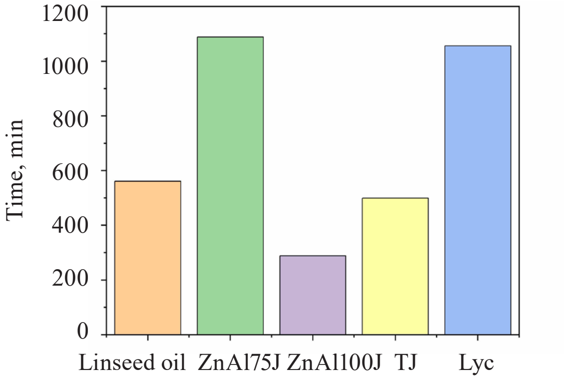

Figure 15 Time to consume ΔPO_2 = 50% of composites and their references at 37°C and 101 KPa. TJ is tomato juice

references slightly decreased in 24 h while all composites and the ZnAl reference increased their activity. ZnAl75J reached 52% inhibition, ZnAl100J reached 64%, and ZnAlLyc reached 82%. Probably, the inorganic particles were the ones contributing to the long-term inhibition, presumably because the Zn and Al oxides/hydroxides slowed down the release of lycopene into the reaction medium.

Antioxidant kinetics with DPPH·. Figure 13 illustrates the kinetics of antioxidant activity. Tomato juice retained 6.6% of the remaining DPPH$^•$ 5 min after the start of the experiment. Due to the fast decay it was not plotted. Using this data as a reference point, we observed that the consumption of DPPH$^•$ decreased rapidly: ZnAl100J consumed 89% of DPPH$^•$ in 23 h (remaining 11%) while ZnAl75J consumed 80% of DPPH$^•$ in 30 h (remaining 20%). Probably, the higher lycopene removal efficiency observed for ZnAl100J indicated that lycopene allowed for greater antioxidant activity in this assay.

In the ABTS$^{•+}$ assay, the composites demonstrated a value of IC_{50} 0.012 µg/mL of ABTS with trolox equivalent antioxidant capacity. All the samples obtained a value higher than that after 5 min of incubation (Fig. 14), indicating a greater antioxidant activity towards ABTS$^{•+}$ than towards DPPH$^•$. This result could be explained by the type and number of charges. In ABTS$^{•+}$, the SO_3^- group had a negative charge. Most likely, this anion was attracted to the charges of zinc or aluminum, just as it happened with the chlorides that shifted the zeta potential to negative values.

In the RapidOxy experiment, the results represented the time required to consume 0.4 mol of O_2, corresponding to ΔP = 50%.

We used purified linseed oil as the oily medium reference in this experiment, which needed 555 min for oxidation. In this experiment, the concentration of linseed oil was 0.03 g/mL. Figure 15 shows that ZnAl75J and lycopene had the longest time of O_2 consumption with 1089 and 1057 min, respectively, which means they provided stronger protection against oxidation. On the other hand, ZnAl100J consumed oxygen faster than tomato juice, taking 287 min. Thus, the protection time was reduced in spite of the fact that this assay had more organic material.

As for the sun protection factor, the values presented in Fig. 16 indicated that ZnAl75J at 15% (SPF 3.08) was the mix with the highest value, followed by ZnAl at 15% (SPF 2.58) and ZnAl100J at 5% (SPF 2.5). Therefore, no high photoprotective synergy occurred between the Zn compounds and the organic material.

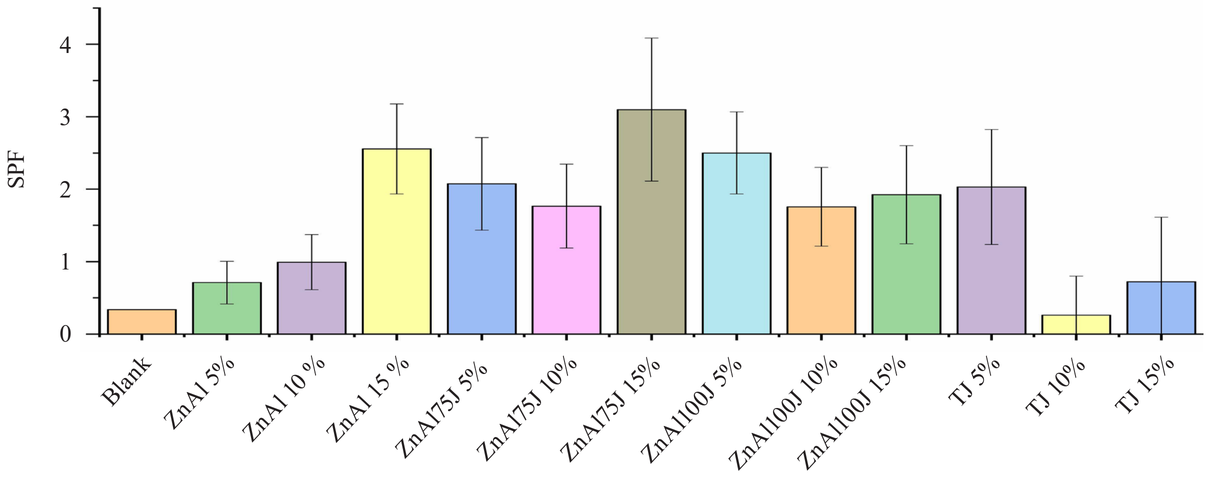

Figure 16 Sun protection factor for composites and references at different concentrations. Each experiment was performed in triplicate, the bars correspond to standard deviations

The sun protection factor values of ZnAl75J and ZnAl100J stayed within the range reported for these compounds [32–34]. Similarly, the sun protection factor of 1 obtained with ZnAl was lower than the values reported for ZnO in [35] as approximately 5 SPF.

Previous studies showed that human skin increases the quantity of carotenoids by approximately 25% during summer and autumn [36]. These composites could then be an alternative to meet the increased need for carotenoids in the skin when applied topically. Corresponding with the obtained zeta potential values, these composites show stability in oil-in-water emulsions [37].

CONCLUSION

The synthesized composites were found to be amorphous, indicating that the reaction did not produce layered double hydroxide crystals when the synthesis was carried out using zinc and aluminum chlorides with tomato juice as a reaction medium. The powdered material was composed of amorphous zinc and aluminum oxides or hydroxides, which removed 97% of the available lycopene in tomato juice under the synthesis conditions of ZnAl100J. Although ZnAl75J removed a smaller amount of lycopene, its antioxidant activity and sun protection factor were sufficient for it to be used as an antioxidant ingredient in food, food packaging, or cosmetics. In addition, its lack of aggregation in water allows for uniform dispersion.

ZnAl100J showed higher antioxidant activity against free radicals while ZnAl75J exhibited the best results for oxidation resistance.

Regarding the sun protection factor, the composites showed no high values; however, they could be considered as substitutes for increasing carotenoids in human skin. Finally, these composites seem to be a promising option for sustainable extraction of lycopene, as well as for encapsulating organic material obtained from tomato juice because they provided protection against degradation and antioxidant loss.

CONTRIBUTIONS

Rosa Nallely Murillo Vázquez designed and conducted the experiments, organized the data, and wrote the draft of the article. Fermín Paul Pacheco Moisés analyzed and processed the results, as well as supervised the work. Verónique Nardello-Rataj provided the conceptualization, supervision, and discussion. Gregorio Guadalupe Carbajal Arízaga provided conceptualization, formal analysis, supervision, and revision.

CONFLICT OF INTEREST

The authors declared no conflict of interests regarding the publication of this article.

ACKNOWLEDGMENTS

The authors acknowledge the technical assistance of José Antonio Rivera Mayorga for collecting the X-ray photoelectron spectra and the Transdisciplinary Institute of Research and Services – ITRANS at the University of Guadalajara for collecting the energy dispersive X-ray spectra. This manuscript is dedicated to the memory of Rosa Nallely Murillo Vázquez, who left this world during the peer review of her manuscript.

INFORMED CONSENT

Informed consent was obtained from all individual participants included in the study.

REFERENCES

1. Heriyanto S, Romulo A. Tomato pomace ketchup: Physicochemical, microbiological, and sensory characteristics. Food Processing: Techniques and Technology. 2023;53(4):766–774. https://doi.org/10.21603/2074-9414-2023-4-2477

2. Madia VN, de Vita D, Ialongo D, Tudino V, de Leo A, Scipione L, *et al.* Recent advances in recovery of lycopene from tomato waste: A potent antioxidant with endless benefits. Molecules. 2021;26(15):4495. https://doi.org/10.3390/molecules26154495
3. Méndez-Carmona JY, Ascacio-Valdes JA, Alvarez-Perez OB, Hernández-Almanza AY, Ramírez-Guzman N, Sepúlveda L, *et al.* Tomato waste as a bioresource for lycopene extraction using emerging technologies. Food Bioscience. 2022;49:101966. https://doi.org/10.1016/j.fbio.2022.101966
4. Yasmeen N, Sameer AS, Nissar S. Lycopene. In: Kour J, Nayik GA, editors. Nutraceuticals and health care. Academic Press; 2022. pp. 115–134. https://doi.org/10.1016/B978-0-323-89779-2.00009-0
5. Hernández DE, Magallon AP, Arizaga GGC. Green extraction of lycopene from tomato juice with layered double hydroxide nanoparticles. Micro and Nano Letters. 2019;14(3):230–233. https://doi.org/10.1049/mnl.2018.5437
6. Chen Z, Fan Q, Huang M, Cölfen H. Synthesis of two-dimensional layered double hydroxides: A systematic overview. CrystEngComm. 2022;24(26):4639–4655. https://doi.org/10.1039/D2CE00511E
7. Min L, Duan J, Song C, Chen Y, Zhang W, Wang Y. Decarbonating layered double hydroxides using a carbonated salt solution. Dalton Transactions. 2023;52(21):7330–7335. https://doi.org/10.1039/D3DT01079A
8. Kesavan Pillai S, Kleyi P, de Beer M, Mudaly P. Layered double hydroxides: An advanced encapsulation and delivery system for cosmetic ingredients – An overview. Applied Clay Science. 2020;199:105868. https://doi.org/10.1016/-j.clay.2020.105868
9. Mosangi D, Moyo L, Kesavan Pillai S, Ray SS. Acetyl salicylic acid-ZnAl layered double hydroxide functional nanohybrid for skin care application. RSC Advances. 2016;6(107):105862–105870. https://doi.org/10.1039/C6RA22172F
10. Cheng H-M, Gao X-W, Zhang K, Wang X-R, Zhou W, Li S-J, *et al.* A novel antimicrobial composite: ZnAl-hydrotalcite with *p*-hydroxybenzoic acid intercalation and its possible application as a food packaging material. New Journal of Chemistry. 2019;43(48):19408–19414. https://doi.org/10.1039/C9NJ03943K
11. Egambaram OP, Kesavan Pillai S, Ray SS, Goosen M. Structural and photoprotective characteristics of Zn-Ti, Zn-Al, and Mg-Al layered double hydroxides – A comparative study. Cosmetics. 2023;10(4):100. https://doi.org/10.3390/cosmetics10040100
12. Szerlauth A, Muráth S, Szilagyi I. Layered double hydroxide-based antioxidant dispersions with high colloidal and functional stability. Soft Matter. 2020;16(46):10518–10527. https://doi.org/10.1039/D0SM01531H
13. Singh A, Ahmad S, Ahmad A. Green extraction methods and environmental applications of carotenoids – A review. RSC Advances. 2015;5(77):62358–62393. https://doi.org/10.1039/C5RA10243J
14. Ma Y, Zhong L, Peng Z, Liu X, Ouyang D, Guan S. Development of a highly water-soluble lycopene cyclodextrin ternary formulation by the integrated experimental and modeling techniques. AAPS PharmSciTech. 2021;22:5. https://doi.org/10.1208/s12249-020-01861-
15. Aghel N, Ramezani Z, Amirfakhrian S. Isolation and quantification of lycopene from tomato cultivated in Dezfoul, Iran. Jundishapur Journal of Natural Pharmaceutical Products. 2011;6(1):9–15.
16. Benítez JJ, Castillo PM, del Río JC, León-Camacho M, Domínguez E, Heredia A, *et al.* Valorization of tomato processing by-products: Fatty acid extraction and production of bio-based materials. Materials. 2018;11(11):2211. https://doi.org/10.3390/ma11112211
17. Gordeeva A, Hsu Y-J, Jenei IZ, Brant Carvalho PHB, Simak SI, Andersson O, *et al.* Layered zinc hydroxide dihydrate, $Zn_5(OH)_{10}\cdot 2H_2O$, from hydrothermal conversion of ε-$Zn(OH)_2$ at gigapascal pressures and its transformation to nanocrystalline ZnO. ACS Omega. 2020;5(28):17617–17627. https://doi.org/10.1021/acsomega.0c02075
18. Bastianini M, Faffa C, Sisani M, Petracci A. Caffeic acid-layered double hydroxide hybrid: A new raw material for cosmetic applications. Cosmetics. 2018;5(3):51. https://doi.org/10.3390/cosmetics5030051
19. Bukhtiyarova MV. A review on effect of synthesis conditions on the formation of layered double hydroxides. Journal of Solid State Chemistry. 2019;269:494–506. https://doi.org/10.1016/j.jssc.2018.10.018
20. Wang T, Jin B, Jiao Z, Lu G, Ye J, Bi Y. Photo-directed growth of Au nanowires on ZnO arrays for enhancing photoelectrochemical performances. Journal of Materials Chemistry A. 2014;2(37):15553–15559. https://doi.org/10.1039/C4TA02960G
21. Chen H, Deng H, Zhong X, Zhou H, Zhan J, Zhou X. Highly dispersed amorphous ZnO on a petal-like porous silica-clay composite with enhanced antimicrobial properties. Colloids and Surfaces B: Biointerfaces. 2022;220:112978. https://doi.org/10.1016/j.colsurfb.2022.112978
22. Xiao S, Zhao L, Leng X, Lang X, Lian J. Synthesis of amorphous TiO_2 modified ZnO nanorod film with enhanced photocatalytic properties. Applied Surface Science. 2014;299:97–104. https://doi.org/10.1016/j.apsusc.2014.01.192

23. Naumkin AV, Kraut-Vass A, Gaarenstroom SW, Powell CJ. NIST X-ray photoelectron spectroscopy database. Gaithersburg: National Institute of Standards and Technology; 2000. https://doi.org/10.18434/T4T88K
24. Rotole JA, Sherwood PMA. Nordstrandite (Al(OH)$_3$) by XPS. Surface Science Spectra. 1998;5:32–38. https://doi.org/10.1116/1.1247854
25. Pooresmaeil M, Behzadi Nia S, Namazi H. Green encapsulation of LDH(Zn/Al)-5-Fu with carboxymethyl cellulose biopolymer; new nanovehicle for oral colorectal cancer treatment. International Journal of Biological Macromolecules. 2019;139:994–1001. https://doi.org/10.1016/j.ijbiomac.2019.08.060
26. Zhang Y, Chang J, Zhao J, Fang Y. Nanostructural characterization of Al(OH)$_3$ formed during the hydration of calcium sulfoaluminate cement. Journal of the American Ceramic Society. 2018;101(9):4262–4274. https://doi.org/10.1111/jace.15536
27. Guo X, Tang M, Wang N, Li L, Wu Y, Chen X, *et al.* The synthesis of organically modified layered double hydroxide and its effect on the structure and physical properties of low-density polyethylene/ethylene–vinyl acetate blends. Polymers and Polymer Composites. 2019;27(5):287–298. https://doi.org/10.1177/0967391119846218
28. Adriany A, Jéssica S, Ana O, Raimunda S, Andreanne V, Luan S, *et al.* Anti-inflammatory and antioxidant activity improvement of lycopene from guava on nanoemulsifying system. Journal of Dispersion Science and Technology. 2021;42(5):760–770. https://doi.org/10.1080/01932691.2020.1728300
29. Cámara M, de Cortes Sánchez-Mata M, Fernández-Ruiz V, Cámara RM, Manzoor S, Caceres JO. Lycopene: A review of chemical and biological activity related to beneficial health effects. Studies in Natural Products Chemistry. 2013;40:383–426. https://doi.org/10.1016/B978-0-444-59603-1.00011-4
30. Guerra AS, Hoyos CG, Molina-Ramírez C, Velásquez-Cock J, Vélez L, Gañán P, *et al.* Extraction and preservation of lycopene: A review of the advancements offered by the value chain of nanotechnology. Trends in Food Science and Technology. 2021;116:1120–1140. https://doi.org/10.1016/j.tifs.2021.09.009
31. Zhang C, Li C, Zhu Y, Cui H, Lin L. Stability of a novel glycosylated peanut protein isolate delivery system loaded with gallic acid. Food Chemistry. 2024;437:137790. https://doi.org/10.1016/j.foodchem.2023.137790
32. Joshi H, Hegde AR, Shetty PK, Gollavilli H, Managuli RS, Kalthur G, *et al.* Sunscreen creams containing naringenin nanoparticles: Formulation development and in vitro and in vivo evaluations. Photodermatology Photoimmunology and Photomedicine. 2018;34(1):69–81. https://doi.org/10.1111/phpp.12335
33. Aloanis AA, Karundeng M, Paat VI, Tengker SMT, Siwu O. Sun protecting factor value of the Ficus benjamina Linn. fruits extract. Journal of Physics: Conference Series. 2021;1968:012009. https://doi.org/10.1088/1742-6596/1968/1/012009
34. Rohmah J, Wulandari FE, Rini CS. In vitro: Sunscreen activity of red lettuce extract (*Lactuca sativa* var. *crispa* L.). IOP Conference Series: Earth and Environmental Science. 2020;519:012009. https://doi.org/10.1088/1755-1315/519/1/012009
35. Fogaça LA, Feuser PE, Ricci-Júnior E, Hermes de Araújo PH, Sayer C, da Costa C. ZnO and quercetin encapsulated nanoparticles for sun protection obtained by miniemulsion polymerization using alternative co-stabilizers. Materials Research Express. 2020;7:015096. https://doi.org/10.1088/2053-1591/ab6c8e
36. Lademann J, Meinke M, Sterry W, Darvin M. Carotenoids in human skin. Experimental Dermatology. 2011;20:377–382. https://doi.org/10.1111/j.1600-0625.2010.01189.x
37. Low LE, Siva SP, Ho YK, Chan ES, Tey BT. Recent advances of characterization techniques for the formation, physical properties and stability of Pickering emulsion. Advances in Colloid and Interface Science. 2020;277:102117. https://doi.org/10.1016/j.cis.2020.102117

ORCID IDs
Rosa Nallely Murillo Vázquez https://orcid.org/0000-0001-7881-6649
Fermín Paul Pacheco Moisés https://orcid.org/0000-0002-3769-5649
Verónique Nardello-Rataj https://orcid.org/0000-0001-8065-997X
Gregorio Guadalupe Carbajal Arízaga https://orcid.org/0000-0003-3120-0243